Error-Feedback Mismatch Error Shaping for High-Resolution Data Converters

Jiaxin Liu, *Student Member, IEEE*, Chen-Kai Hsu, *Student Member, IEEE*, Xiyuan Tang, *Student Member, IEEE*, Shaolan Li, *Student Member, IEEE*, Guangjun Wen, *Senior Member, IEEE*, and Nan Sun, *Senior Member, IEEE*

***Abstract*— Device mismatch is a key concern for high-resolution data converters. This paper presents a comprehensive study of the error-feedback (EF)-based mismatch error shaping (MES) technique. EF MES overcomes the key challenge of the classic dynamic element matching-based MES whose complexity grows exponentially with the number of bits; however, the prior EF MES comes with the limitations of limited shaping capability and reduced dynamic range. This paper demonstrates how to perform more advanced EF MES for various types of data converters. Moreover, this paper also proposes the use of digital prediction to address the dynamic range loss issue.**

***Index Terms*— Analog-to-digital converter (ADC), digital-to-analog converter (DAC), successive approximation register (SAR), error-feedback (EF), mismatch error shaping (MES), dynamic element matching (DEM), ADC with prediction.**

I. Introduction

DEVICE mismatch is typically the linearity bottleneck for multi-bit analog-to-digital converters (ADCs) and digital-to-analog converters (DACs). A classic solution to address mismatch is to use calibration [1]–[3]. The merit of calibration is that it can completely remove the mismatch error, but the limitation is that it requires the mismatch error to be measured and compensated precisely (even more accurate than the nominal ADC/DAC resolution), which is nontrivial in practical implementation. In addition, the mismatch error may drift due to environment changes (e.g., temperature variation and aging). It requires repeated calibration, which may interrupt the normal ADC/DAC operation. One way to address this problem is to use background calibration that can track component variations [4]–[6]. Nevertheless, the price is the increased hardware cost (power, area and complexity). Also, background calibration may take a long time to converge, and thus, is unsuitable for single-shot or short-term measurements.

Another method to address the mismatch problem is to use dynamic element matching (DEM). The rationale of DEM is not to remove the mismatch error, but rather spectrally shape it in such a way that it does not affect the overall linearity. In implementation, DEM requires the DAC to be decomposed into equally weighted unit elements. An element selection logic (ESL) block is used to randomly select the unity-weighted DAC elements at every clock cycle. Even though the mismatch errors still exist, they are averaged out over time. An early DEM technique of [7] show that the DAC mismatch error can be turned into white noise. By barrel-shifting the DAC elements, the data-weighted averaging (DWA) based DEM can achieve the 1st-order mismatch shaping [8]–[11]. Lately, advanced mismatch shaping techniques can achieve higher-order shaping [12]–[15]. Comparing to calibration, the merit of DEM is that it does not need any prior knowledge of the mismatch error, and thus, it does not require any extra circuitry for precise analog error measurement and compensation. By contrast, its ESL block is purely digital, and thus, scaling friendly. Nevertheless, DEM comes with its own limitations. Its ESL block introduces extra delay, which is undesirable for a high-speed closed-loop system (e.g., a $\Delta\Sigma$ ADC). If the DAC digital input is binary sequences (e.g., from a SAR quantizer), an additional binary-to-thermometer decoder is needed, which further elongates the delay. In addition, DEM increases the element switching rate and can cause large dynamic errors for continuous-time ADCs/DACs [16], [17]. Furthermore, a critical limitation for the classic DEM is that the number of independently-addressable unity-weighted DAC elements grow exponentially with the DAC resolution, making the hardware cost too high when it is directly applied in a high-resolution data converter without segmentation. However, many applications demand high-resolution data converters to reduce the quantization error. For example, many SAR ADCs are more than 10-bit. The recently emerging noise-shaping SAR ADCs also have 7-bit or higher resolution [18]–[25].

There are two methods to address the DEM's complexity problem for high-resolution data converters. One method

Manuscript received June 21, 2018; revised September 5, 2018, September 28, 2018, and October 30, 2018; accepted October 31, 2018. Date of publication November 28, 2018; date of current version March 15, 2019. This work was supported by the National Natural Science Foundation of China under Project Contracts 61371047 and 61601093. This paper was recommended by Associate Editor P. Rombouts. *(Corresponding author: Jiaxin Liu.)*

J. Liu is with the School of Information and Communication Engineering, University of Electronic Science and Technology of China, Chengdu, Sichuan 611731, China, with the Department of Electrical and Computer Engineering, The University of Texas at Austin, Austin, TX 78712 USA, and also with the Department of Electronic Engineering, Tsinghua University, Beijing 100084, China (e-mail: jiaxin.liu@ieee.org).

C.-K. Hsu, X. Tang, S. Li, and N. Sun are with the Department of Electrical and Computer Engineering, The University of Texas at Austin, Austin, TX 78712 USA, and also with Tsinghua University, Beijing 100084, China (e-mail: nansun@mail.utexas.edu).

G. Wen is with the School of Information and Communication Engineering, University of Electronic Science and Technology of China, Chengdu 611731, China (e-mail: wgj@uestc.edu.cn).

Color versions of one or more of the figures in this paper are available online at http://ieeexplore.ieee.org.

Digital Object Identifier 10.1109/TCSI.2018.2879582

1549-8328 © 2018 IEEE. Personal use is permitted, but republication/redistribution requires IEEE permission.
See http://www.ieee.org/publications_standards/publications/rights/index.html for more information.

Authorized licensed use limited to: Tsinghua University. Downloaded on February 21,2020 at 14:14:43 UTC from IEEE Xplore. Restrictions apply.

is to apply DEM only to the most-significant-bit (MSB) bits [22], [23]. The partial DEM is feasible because the MSB bits contribute the bulk of the mismatch error. Take a 12-bit DAC as an example, we only apply DEM to the first 4-bits. This substantially lowers the hardware complexity. It removes the MSB mismatch errors, but it cannot address the least-significant-bit (LSB) mismatch errors. As a result, it is insufficient for applications that demand high linearity, especially when the input is small [21]. The other method to reduce complexity is to use segmented DEM [26]–[31]. Unlike the classic DEM which operates with unity-weighted elements, segmented DEM avoids the exponential hardware complexity by manipulating DAC segments with different element weights. As long as sufficient redundancy is retained for the input values, harmonic distortions from element mismatch can be avoided. However, the redundancy causes dynamic range loss. For instance, a 14-bit DAC with the fully segmented DEM in [27] can be free of nonlinear distortion with only 28 elements, but it requires a maximal total element weight of 2^{15}, corresponding to a worst-case dynamic range loss of 6 dB. The highly-segmented DEM technique in [28] can reduce the dynamic range loss to 1.2 dB as the total element weight required for a 14-bit DAC is reduced to 18430, however it increases the number of required DAC elements to 36.

Recently, Shu *et al.* [21] developed a mismatch error shaping (MES) technique that can address many aforementioned limitations of existing DEM techniques. It is based on a different concept. Unlike DEM that relies on element scrambling, this MES technique of [21] works by explicitly feeding back the mismatch errors from the previous conversion cycle and subtracting them out in the present conversion cycle. In this paper, we call it the error-feedback (EF) MES technique based on its operation principle, and to differentiate it from the classic DEM based MES techniques. The hardware complexity of EF MES is low and grows only linearly with the DAC resolution. EF MES can be realized simply by delaying the reset of the LSB capacitors. It does not require any ESL block or binary-to-thermometer encoder as in DEM MES. Moreover, EF MES can be directly applied to a power-of-two-weighted DAC without any modification. By contrast, the classic DEM MES requires decomposing the M-bit power-of-two-weighted DAC into 2^M unity-weighted elements; even the fully segmented DEM of [27] still requires $2M$ DAC elements. Hence, the hardware cost of EF MES is much smaller than that of DEM MES, making it well suited for high-resolution data converters.

Despite clear advantages, the original EF MES scheme of [21] has its limitations. First, the original form of EF MES presented in [21] can only achieve 1st-order MES and suffers from idle tones. It cannot be directly generalized to higher-order and more advanced shaping forms. Second, the feedback of all LSB DAC values eats up the input signal range, causing 6 dB dynamic range loss. To alleviate this issue, the work of [21] separates the DAC into a thermometer MSB segment and a power-of-two-weighted LSB segment, and separately applies DEM MES and EF MES to each of them. This, however, increases the hardware complexity and brings back the necessity of a thermometer DAC, an ESL block and a binary-to-thermometer encoder, sacrificing the benefits of EF MES. Even so, it only minimizes but not eliminates the dynamic loss.

This paper presents a comprehensive study of EF MES and proposes several novel techniques to address the limitations of the prior EF MES technique of [21]. Building upon our prior work of [32], this paper systematically generalizes EF MES to 2nd-order and other more advanced forms, enabling it to be applied to various types of low-pass, band-pass, and high-pass converters. Moreover, it addresses the critical dynamic range loss problem by using digital prediction and taking advantage of the tri-level nature of the MSB capacitor in a fully-differential DAC. By using advanced prediction schemes, the proposed technique can support full-scale signal range with only a mild oversampling ratio of 2, which is commonly supported by both Nyquist and oversampling data converters. The need for a separate thermometer DAC segment is eliminated, greatly reducing circuit complexity.

In this paper, we take a 16-bit SAR ADC to illustrate the proposed techniques. It is noted that these techniques are generally applicable for other power-of-two-weighted ADCs and DACs. This paper is organized as follows. Section II reviews the prior EF MES technique of [21]. Section III generalizes EF MES to 2nd-order shaping and other forms. Section IV proposes the prediction techniques to address the dynamic range loss issue. Finally, Section V concludes the paper.

II. Review of Prior EF MES Technique

A. Definition of Mismatch Error in SAR ADC

Fig. 1(a) shows a conventional 16-bit SAR ADC. The MSB capacitor C_{15} is used as a reference. Each LSB capacitor has a mismatch e_i when referring to C_{15}:

$$e_i \equiv C_i - 2^i C = C_i - 2^i \cdot \frac{C_{15}}{2^{15}} \tag{1}$$

D_i is the digital control code (± 1) for each capacitor C_i after conversion. Behaviorally, the SAR ADC operation can be modeled as in Fig. 1(b). In the analog domain, the weight of the MSB capacitor, $DAC_{MSB} = D_{15} \cdot C_{15}/C_{tot}$, and the weight sum of the LSB capacitors, $DAC_{LSB} = \sum_{i=0}^{14} D_i \cdot C_i/C_{tot}$, are sequentially subtracted from the analog input V_i to bring it close to 0, where $C_{tot} = \sum_{i=0}^{15} C_i$.

Along with the subtraction of DAC_{LSB}, the DAC mismatch error E is introduced in the signal path. In the digital domain, the digital output D_o is constructed by adding up the digital weight of the MSB, D_{MSB}, and the LSB weights, D_{LSB}. As a result, D_o is given by

$$D_o = D_{MSB} + D_{LSB} = V_i - E \tag{2}$$

where $D_{MSB} = D_{15}/2$ and $D_{LSB} = \sum_{i=0}^{14} D_i \cdot 2^{i-16}$. E is given by:

$$E = \frac{\sum_{i=0}^{14} D_i \cdot e_i}{C_{tot}} \tag{3}$$

Using this definition, both V_i and D_o are in the range of $[-1, +1]$. Here, the quantization error and noise are ignored for simplicity purpose to focus the discussion on the mismatch error E.

Authorized licensed use limited to: Tsinghua University. Downloaded on February 21,2020 at 14:14:43 UTC from IEEE Xplore. Restrictions apply.

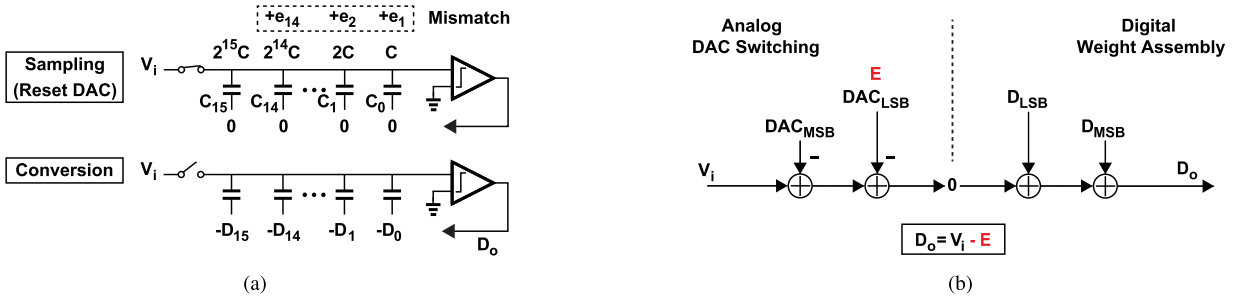

Fig. 1. Illustration of SAR ADC with DAC mismatch: (a) Switching scheme and (b) behavioral model.

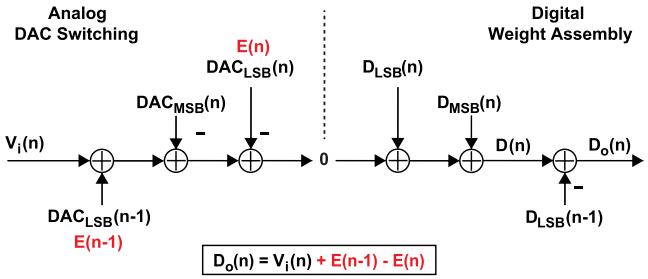

Fig. 2. Behavioral model of SAR ADC with EF MES [21].

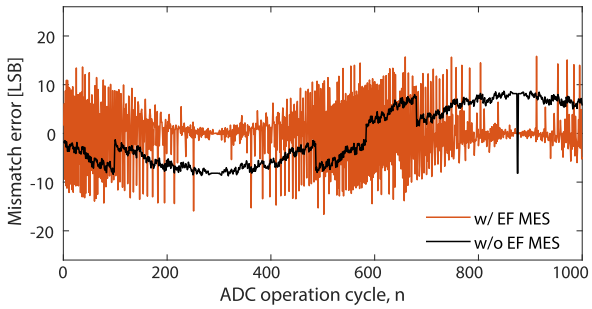

Fig. 3. Simulated mismatch error waveforms of a 16-bit SAR ADC with and without EF MES.

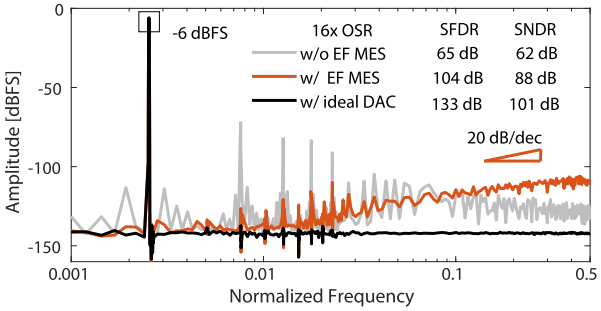

Fig. 4. Simulated output spectra of a 16-bit SAR ADC with and without EF MES.

B. Prior EF MES Technique of [21]

The prior EF MES technique of [21] works by feeding back the mismatch error of the previous conversion cycle, $E(n-1)$, to the present cycle as shown in Fig. 2. It can be implemented simply by maintaining the previous LSB capacitor connections during the sampling phase and resetting them in a separate reset phase. In this way, $E(n-1)$ is fed back to the input along with the previous cycle LSB values $DAC_{LSB}(n-1)$. As a result, $D_{LSB}(n-1)$ has to be subtracted out from $D(n) \equiv D_{MSB}(n) + D_{LSB}(n)$ to get the correct digital output $D_o(n)$, which is given by:

$$D_o(n) = D(n) - D_{LSB}(n-1) = V_i(n) + E_{tot}(n) \quad (4)$$

where the total mismatch error $E_{tot}(n)$ is given by:

$$E_{tot}(n) = E(n-1) - E(n) \quad (5)$$

which clearly shows the 1st-order shaping.

Fig. 3 shows the DAC mismatch error waveforms with and without the 1st-order EF MES. Without EF MES, the original mismatch error is highly correlated with the input, leading to large distortions. With EF MES, because of the dither-like LSB injection, the DAC mismatch error is randomized. Moreover, due to the mismatch error subtraction, the low-frequency components are canceled out and the high-frequency components are overlaid, leading to the greatly reduced signal dependence but the twice bigger worst-case errors.

However, one limitation of the 1st-order EF MES is that its mismatch shaping capability is limited, which is insufficient for applications where both linearity and area requirements are stringent. Fig. 4 shows the behaviorally simulation results of a 16-bit SAR ADC with 1st-order EF MES. The mismatch among unit capacitors is assumed to follow the normal distribution with a standard deviation of $\sigma = 5\%$. The thermal noise power is assumed to be equal to that of the quantization error. It can be seen that the performance is significantly improved after enabling the EF MES, but the spectrum still has obvious harmonic distortions. Comparing to SAR ADC with an ideal DAC, the SFDR and SNDR drops are 29 dB and 13 dB, respectively, at the OSR of 16. This is because 1st-order mismatch shaping still has appreciable signal dependence and can produce considerable harmonic distortions. Besides, because the LSB feedback is deterministic, the 1st-order EF MES is prone to produce high-frequency spurs, especially when OSR is small.[1] Thus, it is desirable to develop novel EF MES techniques that can achieve more advanced high-order mismatch shaping.

Another critical limitation of the EF MES of [21] is that it suffers from dynamic range loss. For the standalone EF MES illustrated in Fig. 2, the value of LSB feedback,

[1]The classic DWA also suffers from high-frequency spurs [8]–[11], and this issue can be mitigated by advanced DEM techniques [33], [34].

Authorized licensed use limited to: Tsinghua University. Downloaded on February 21,2020 at 14:14:43 UTC from IEEE Xplore. Restrictions apply.

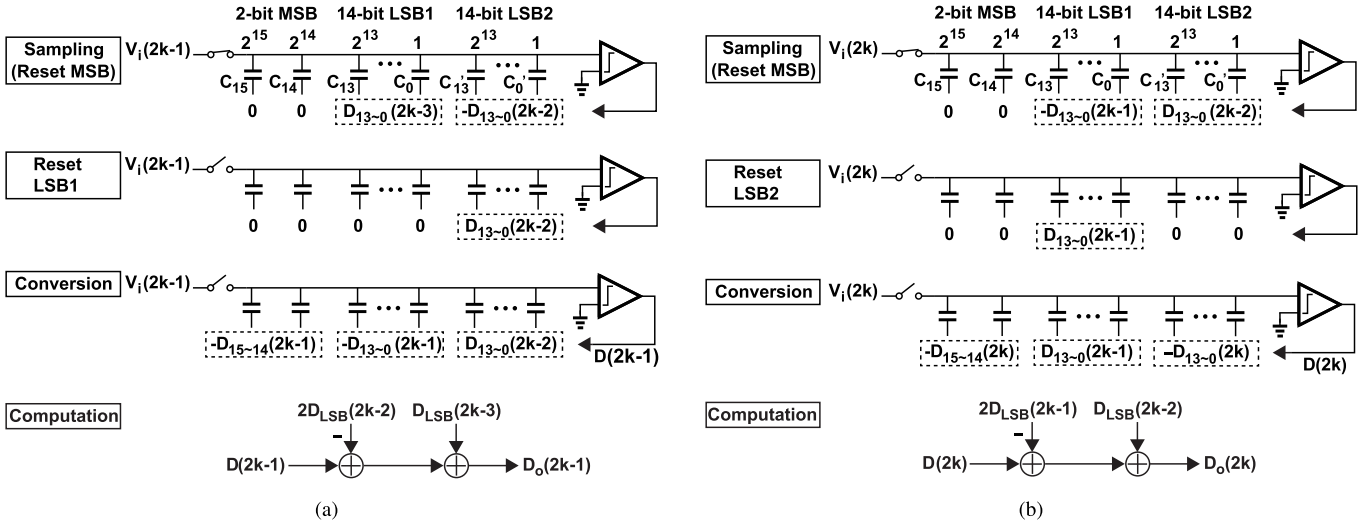

Fig. 5. Implementation of SAR ADC with proposed 2nd-order EF MES in (a) odd cycle and (b) even cycle [32].

$DAC_{LSB}(n-1)$, consumes a signal range of 1/2 full-scale. To prevent ADC from saturation, the analog input signal, V_i has to be reduced by half, resulting 6 dB dynamic range loss. This is a significant dynamic range penalty. The work of [21] alleviates this issue by segmenting the DAC into a thermometer MSB section and a power-of-two-weighted LSB section, and apply DEM and EF MES separately. However, this comes with the cost of increased hardware complexity. It brings back the limitations of DEM that EF MES aims to address, including the need for the ESL, the binary-to-thermometer encoder, and the increased delay. In addition, the dynamic range loss still exists, though reduced from 6 dB to 1.2 dB as in [21].

III. Proposed EF MES With 2nd-Order Shaping and General Form

In [32], we proposed the 2nd-order EF MES with high-pass filtering for SAR ADCs. In this section, we discuss the 2nd-order EF MES in detail with comprehensive simulations, and compare it to the 1st-order one to show its advantage of higher linearity enhancement capability. Furthermore, we provide general EF MES solutions for various types of low-pass, band-pass, and high-pass applications.

A. 2nd-Order EF MES

Inspired by the 1st-order EF MES, a clear way to realize the 2nd-order one is to feed back a combination of previous mismatch errors, $2E(n-1)-E(n-2)$. To this end, a combination of LSB analog weights from previous two cycles, $2DAC_{LSB}(n-1)-DAC_{LSB}(n-2)$, needs to be fed to the ADC input before the SAR conversion starts. Note that directly applying the digital sum, $2D_{LSB}(n-1)-D_{LSB}(n-2)$, to the LSB DAC does not work, as the DAC mismatch error is no longer $2E(n-1)-E(n-2)$ but replaced by a new one determined by the pattern of the digital sum. Instead, to keep $2E(n-1)-E(n-2)$ unchanged, $2DAC_{LSB}(n-1)$ and $DAC_{LSB}(n-2)$ need to be fed back independently. The challenge is that how to handle so many independent values in a single ADC operation cycle.

We proposed a scheme that realizes the 2nd-order EF MES in [32] by employing two LSB DACs, as shown in Fig. 5. A 2-bit MSB is used to prevent the ADC from being saturated by the LSB feedback, which will be discussed in detail later. The two LSB DACs operate in a ping-pong fashion to convert the input signal.

Without EF MES, the mismatch error introduced in a ADC operation cycle, n, can be expressed as

$$E(n)=\begin{cases}-E_1(n), & n=2k-1\\ -E_2(n), & n=2k.\end{cases} \tag{6}$$

where E_1 and $E2$ are the mismatch errors from LSB1 and LSB2, respectively. The MSB DAC is assumed to have no mismatch in the analysis. In a practical design, the MSB mismatch can be addressed by using an extra DEM [21].

With the proposed 2nd-order EF MES, the total mismatch error introduced in a ADC operation cycle, n, becomes [32]

$$E_{tot}(n)=\begin{cases}-E_1(n)+2E_2(n-1)-E_1(n-2), & n=2k-1\\ -E_2(n)+2E_1(n-1)-E_2(n-2), & n=2k\end{cases} \tag{7}$$

From (6) and (7), we can obtain the following relationship

$$E_{tot}(n)=E(n)-2E(n-1)+E(n-2). \tag{8}$$

It shows that $E_{tot}(n)$ is the 2nd-order difference of $E(n)$. As $E(n)$ is a bounded sequence, we can conclude that $E_{tot}(n)$ must be 2nd-order high-pass shaped [35].

Fig. 6 shows the waveforms of DAC mismatch errors with and without the 2nd-order EF MES. Without EF MES, the original mismatch error waveform shows obvious low-frequency patterns. After enabling the 2nd-order EF MES, these low-frequency patterns are eliminated and shaped to high-frequency noise.

Fig. 7 shows the simulated output spectra of the 16-bit SAR ADC with and without the proposed 2nd-order EF MES.

Authorized licensed use limited to: Tsinghua University. Downloaded on February 21,2020 at 14:14:43 UTC from IEEE Xplore. Restrictions apply.

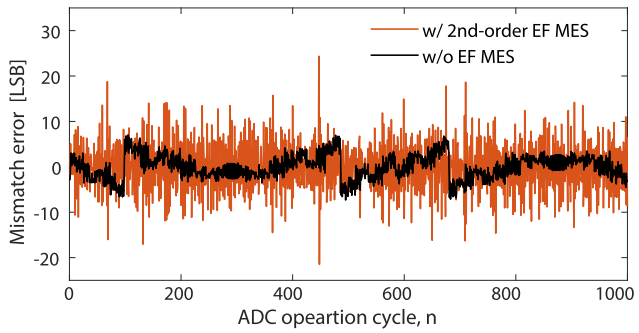

Fig. 6. Simulated mismatch error waveforms of a 16-bit SAR ADC with and without 2nd-order EF MES.

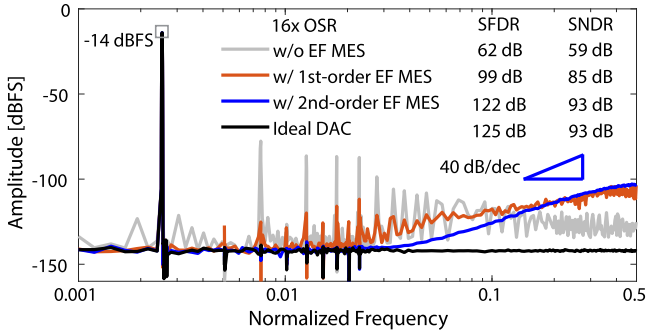

Fig. 7. Simulated output spectra of a 16-bit SAR ADC with and without 2nd-order EF MES.

The mismatch among unit LSB DAC cells is assumed to follow the normal distribution with a standard deviation of $\sigma = 5\%$. The ADC input amplitude is set to -14 dBFS to avoid saturation after applying the 2nd-order EF MES, which will be addressed later. Comparing to the 1st-order EF MES, the 2nd-order EF MES achieves 23 dB more SFDR and 8 dB more SNDR, at $16\times$ OSR. Moreover, owing to the randomness added by the ping-pong feedback from two LSB DACs and the aggressive shaping capability by the proposed 2nd-order EF MES, its spectrum shows no appreciable spurious tones and the 40dB/dec slope in high-frequencies. Comparing to the ideal DAC case, there is only a slight SFDR drop of 3 dB.

Nevertheless, comparing to the 1st-order EF MES, a drawback of the 2nd-order one in Fig. 5 is that it increases the amount of unit capacitors by 25%. Thus, for the same unit capacitor size, the DAC switching energy is increased by 25%; for the same total DAC size, the unit capacitor mismatch is increase by 12%. In a practical design, the latter can be a preferred option as the 2nd-order EF MES provides much stronger shaping capability. Besides, the 2nd-order EF MES requires two M-bit adders to compute the final result, while only one adder is required by the 1st-order EF MES.

B. General Form of EF MES

The 1st-order high-pass EF MES with transfer function of $1-z^{-1}$ is achieved by feeding back the previous LSB. It also has been shown in [21] that the $1+z^{-1}$ EF MES can be achieved by feeding back the inverted previous LSB and the $1+z^{-2}$ EF MES is realized by feeding back the inverted LSB from two cycles ago. Moreover, we propose the 2nd-order $(1-z^{-1})^2$ EF MES by employing two LSB DACs operating in a ping-pong fashion to feed back $2D_{LSB}(n-1)-D_{LSB}(n-2)$. Following this concept, one can expect that more types of EF MES are available.

The behavioral model of our proposed general form of EF MES is illustrated in Fig. 8. A series of previous DAC mismatch errors, $-c_1E(n-1),\cdots,-c_iE(n-i),\cdots,-c_kE(n-k)$ are fed to the ADC input to cancel the present DAC mismatch error, $E(n)$. By doing this, the final total mismatch error becomes

$$E_{tot}(n) = E(n) + c_1E(n-1) + \cdots + c_iE(n-i) + \cdots + c_kE(n-k). \quad (9)$$

The resulted transfer function of the general form of EF MES can be expressed as

$$TF_{MES} = 1 + c_1z^{-1} + \cdots + c_iz^{-i} + \cdots + c_kz^{-k}. \quad (10)$$

In order to feed back the multiple independent DAC mismatch errors in a single ADC operation cycle, multiple LSB DACs are required. Fig. 9 presents the implementation of our proposed general form of EF MES. The $(M+N)$-bit DAC is segmented with a M-bit MSB DAC and multiple N-bit LSB DACs.

The multiple LSB DACs operate in a time-interleaved manner. Their corresponding DAC mismatch errors are fed back in the sampling and reset phases. The coefficients $a_1 \sim a_k$ control the DAC switchings in the sampling phase and $b_1 \sim b_k$ control those in the reset phase. In this way, the DAC mismatch error on a certain LSB DAC can be fed back twice in a single SAR operation cycle. The coefficients $c_1 \sim c_k$ in (10) are realized by

$$c_i = a_i - b_i, \quad i = 1, 2, \cdots, k. \quad (11)$$

where $a_i, b_i \in \{-1, 0, 1\}$. It is noted that $b_k = 0$, because the LSB DAC controlled by the digital codes from k cycles ago, $D_{(N-1)\sim0}(n-k)$, needs reset to 0 and then performs the SAR conversion. From (11), it is clear that

$$c_i \in \begin{cases} \{-2,-1,0,1,2\}, & i = 1,2,\cdots,k-1 \\ \{-1,0,1\}, & i = k. \end{cases} \quad (12)$$

The restriction on c_i is a limitation of the general form of EF MES. It can only realize limited forms of high-pass and low-pass EF MES, which are $1-z^{-1}$, $(1-z^{-1})^2$, $1+z^{-1}$, $(1+z^{-1})^2$. However, it can provide a variety of complex EF MES solutions with bandpass shaping. For example, it can realize $1+z^{-2}$ with a pair of zeros at $\pm f_s/4$ [21], $1+z^{-1}+z^{-2}$ with a pair of zeros at $\pm f_s/3$, $1+2z^{-1}+2z^{-2}+z^{-3}$ with three zeros at $\pm f_s/3$ and $f_s/2$.

In Fig. 9, it shows that there are k LSB DACs for implementing the EF MES transfer function with up to z^{-k} term. Actually the number of LSB DACs, k^*, may be smaller than k, it depends on the specific LSB feedback terms. For example, the $1+z^{-2}$ EF MES requires only one LSB DAC because only one LSB term needs to be fed back; the $1+z^{-1}+z^{-2}+z^{-3}$ EF MES requires only two LSB DACs because the z^{-1} and z^{-3}

Authorized licensed use limited to: Tsinghua University. Downloaded on February 21,2020 at 14:14:43 UTC from IEEE Xplore. Restrictions apply.

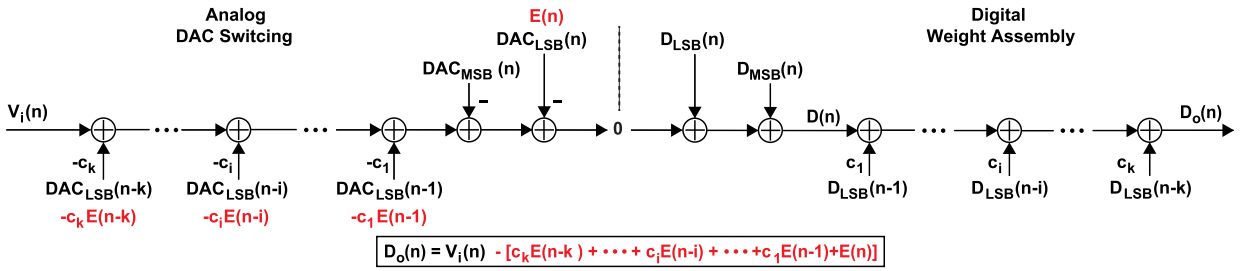

Fig. 8. Behavioral model of SAR ADC with of EF MES.

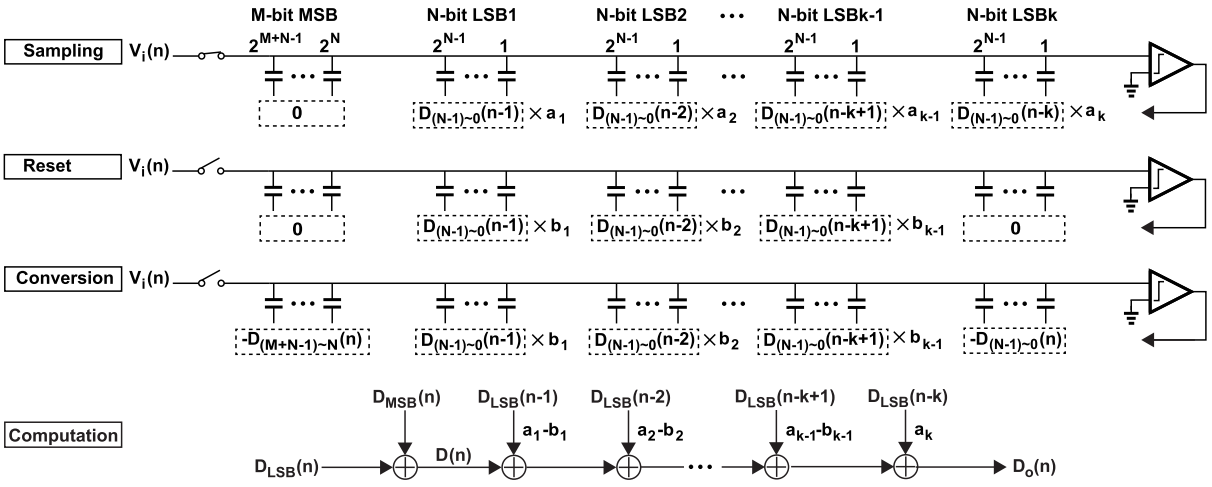

Fig. 9. Implementation of SAR ADC with general form of EF MES.

terms can be fed back through a same LSB DAC in the sampling and reset phases, respectively.

A multi-bit MSB can be necessary to prevent ADC from being saturated by the LSB feedback. For the segmented DAC with a M-bit MSB and k^* LSB DACs, the maximum signal swing that can be processed without saturating the ADC is

$$A_{max} = \frac{2^M}{2^M - 1 + k^*}. \tag{13}$$

The signal range occupied by the LSB feedback is

$$A_{LSB} = \frac{\sum_{i=1}^{k} |c_i|}{2^M - 1 + k^*}. \tag{14}$$

Thus, the available input signal swing can be obtained as

$$A_{in} = A_{max} - A_{LSB} = \frac{2^M - \sum_{i=1}^{k} |c_i|}{2^M - 1 + k^*}. \tag{15}$$

The minimum bit of MSB is determined by the inequation, $A_{in} > 0$, which can be translated into

$$M > \log_2 \left(\sum_{i=1}^{k} |c_i| \right) \tag{16}$$

this requirement on M ensures that the ADC will not be saturated by the LSB feedback.

IV. Addressing Dynamic Range Loss by Prediction

From the discussions above, we know that the standalone 1st-order EF MES MES suffers from 6 dB dynamic range loss. By equation (15), we can figure out the input signal swing for 2nd-order EF MES with a 2-bit MSB is 0.2, corresponding to a dynamic range loss of 14 dB. Using segmented DAC with larger bit of MSB can reduce the dynamic range loss. In [21], the dynamic range loss by 1st-order EF MES is reduced to 1.2 dB with a 3-bit segmented MSB. According to (15), the dynamic range loss by 2nd-order EF MES can be reduced to 5.1 dB or 2.3 dB with a 3-bit or 4-bit MSB, respectively. However, it is at the price of the exponentially increased circuit complexity for an extra DEM to address the MSB mismatch. Even so, the dynamic range loss still exists. To mitigate this trade-off, we propose to use prediction to address the dynamic range loss and relax the requirement on the segmented MSB bit.

A. Basic Form of Prediction: 1-Bit 1st-Order Prediction

In the original EF MES work of [21], $DAC_{LSB}(n-1)$ is added to the input during the sampling phase, the MSB capacitor is always connected to 0 (i.e., common mode). As a result, the total effective ADC input, $V_{i,eff}$, is given by:

$$V_{i,eff}(n) = V_i(n) + DAC_{LSB}(n-1) \tag{17}$$

Authorized licensed use limited to: Tsinghua University. Downloaded on February 21,2020 at 14:14:43 UTC from IEEE Xplore. Restrictions apply.

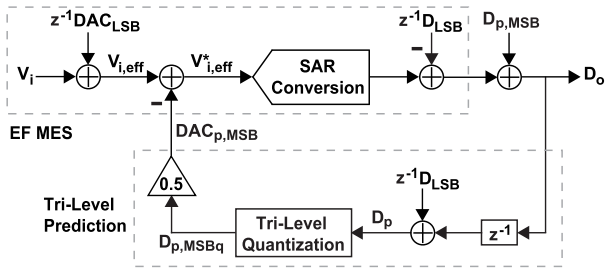

Fig. 10. Proposed EF MES with tri-level prediction.

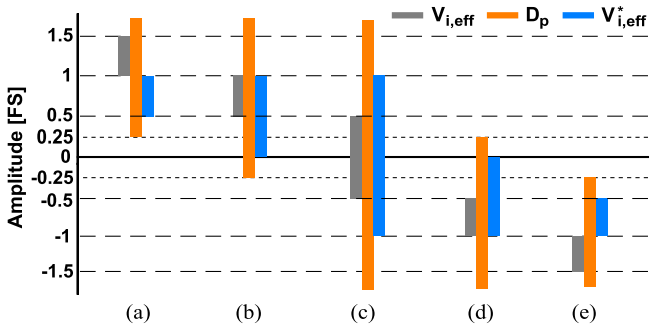

Fig. 11. Relationship between $V_{i,eff}$, D_P, and $V^*_{i,eff}$ under different conditions (a) $1 < V_{i,eff} < 1.5$; (b) $0.5 < V_{i,eff} \leq 1$; (c) $-0.5 < V_{i,eff} \leq 0.5$; (d) $-1 < V_{i,eff} \leq -0.5$; and (e) $-1.5 < V_{i,eff} \leq -1$.

Thus, if $V_i(n)$ and $DAC_{LSB}(n-1)$ have the same polarity, it can cause over range. The signal range of $V_{i,eff}(n)$ is $[-1.5, +1.5]$.

The proposed technique makes use of the MSB capacitor, C_{MSB}, to form a tri-level prediction of $V_{i,eff}(n)$ and subtract it out, as illustrated in Fig. 10. Mathematically speaking, in the proposed scheme, a new effective ADC input for SAR conversion is defined as:

$$V^*_{i,eff}(n) = V_{i,eff}(n) - DAC_{p,MSB}(n) \tag{18}$$

where $DAC_{p,MSB}(n)$ is the value subtracted from $V_{i,eff}(n)$ through the MSB capacitor, $DAC_{p,MSB}(n) \in \{-C_{MSB}/C_{tot}, 0, C_{MSB}/C_{tot}\} \approx \{-0.5, 0, 0.5\}$. As a result, as long as $DAC_{p,MSB}(n)$ is a reasonably good approximation for $V_{i,eff}(n)$, $V^*_{i,eff}(n)$ can be maintained within the signal range of $[-1, +1]$.

By examining (17), it is obvious that $DAC_{LSB}(n-1)$ can be directly obtained from the previous LSB conversion result $D_{LSB}(n-1)$, and thus, is known. However, $V_i(n)$ is the input of the present conversion cycle, and is unknown. To address this issue, we can use digital prediction [36], [37]. The most straightforward prediction is to use the previous conversion result $D_o(n-1)$ to approximate $V_i(n)$. This assumes a reasonable oversampling, such that there exists correlation between $V_i(n-1)$ and $V_i(n)$.

Mathematically speaking, the digital prediction $D_p(n)$ for $V_{i,eff}(n)$ is given by:

$$D_p(n) = D_o(n-1) + D_{LSB}(n-1) \tag{19}$$

Thus, the prediction error $E_p(z)$ is given by:

$$E_p(z) \equiv V_{i,eff}(z) - D_p(z) \approx V_i(z) \cdot (1 - z^{-1}) \tag{20}$$

This shows that $E_p(z)$ is essentially a 1st-order high-pass filtering of $V_i(z)$. Note that $D_p(n)$ is multi-bit, and thus, cannot be directly applied to the MSB capacitor, which can only accept the value of $\{-1, 0, +1\}$. Thus, a tri-level quantization has to be performed on $D_p(n)$, as follows:

$$D_{p,MSBq} = \begin{cases} -1, & \text{for } D_p < -0.25 \\ 0, & \text{for } -0.25 \leq D_p \leq 0.25 \\ +1, & \text{for } D_p > 0.25 \end{cases} \tag{21}$$

where $D_{p,MSBq}$ is the connection of the MSB capacitor during the sampling phase. The quantization threshold is chosen to be 0.25 to support the largest input frequency and amplitude without saturation.

Finally, to compensate for the additional $DAC_{p,MSB}$ subtracted from the input, the digital weight of $DAC_{p,MSB}$ is added up to the digital output, which is given by

$$D_o(n) = D(n) - D_{LSB}(n-1) + D_{p,MSB}(n) \tag{22}$$

where $D_{p,MSB} = D_{p,MSBq}/2$.

Fig. 11 shows the relationship between $V_{i,eff}$, D_p, and $V^*_{i,eff}$. Depending on the range of $V_{i,eff}$, the requirement on D_p to ensure $V^*_{i,eff} \in [-1, +1]$ is different. It can be divided into 5 different cases. When $V_{i,eff} \in [1, 1.5]$, D_p has to be greater than 0.25 to make $V^*_{i,eff} \in [0.5, 1]$. When $V_{i,eff} \in [0.5, 1]$, D_p has to be greater than -0.25 to make $V^*_{i,eff} \in [0, 1]$. When $V_{i,eff} \in [-0.5, +0.5]$, there is no requirement on D_p as $V^*_{i,eff}$ is guaranteed to be within $[-1, +1]$ even when the prediction is wrong. When $V_{i,eff}$ is negative, the requirement is simply the mirrored version for the positive cases. Based on these requirements, we can derive that the maximally allowed prediction error E_p can be as large as 0.75, which is easy to satisfy.

Fig. 12(a) shows the hardware implementation of the proposed EF MES technique with prediction when applied to the 16-bit SAR ADC. Comparing to the original EF MES scheme of [21], the key difference is that the predicted $D_{p,MSBq}(n)$ is connected to C_{15} during the sampling phase to reduce the effective input signal range. Besides, it requires additional digital circuits for the additions of $D_{p,MSB}(n)$ and $D_{LSB}(n-1)$, and a tri-level quantization. Fig. 12(b) shows the timing diagram. Comparing to the original form of EF MES in [21], the proposed EF MES with prediction requires two extra clock phases for computing the final digital output and making the prediction, which cause speed degradation. However, because the computation and prediction are simple, the amount of time needed is small. Note that this minor speed penalty can be avoided by embedding the prediction operation within the SAR conversion phase as shown in Fig. 12(c). The prediction can be done only using the MSB SAR conversion results, and thus, it can be performed simultaneously with the SAR LSB comparisons. Note that doing prediction with only a few MSB bits will cause the slight increase of the prediction error; however, because the error is only at the last several LSB levels, its impact is small.

Authorized licensed use limited to: Tsinghua University. Downloaded on February 21,2020 at 14:14:43 UTC from IEEE Xplore. Restrictions apply.

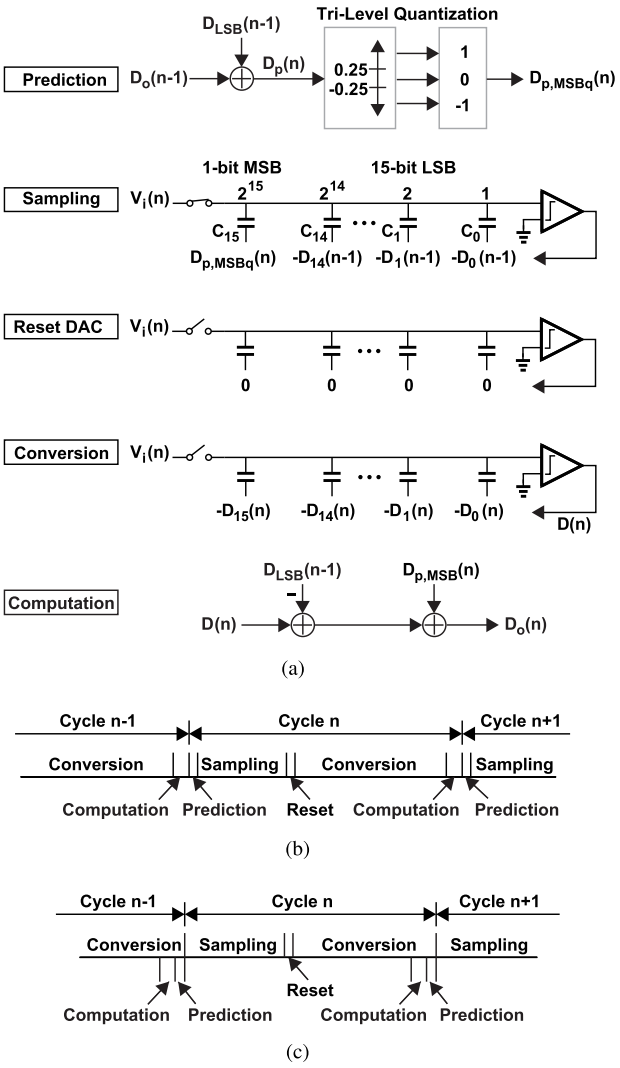

Fig. 12. Implementation of EF MES with prediction. (a) SAR ADC operation, (b) timing diagram and (c) timing diagram of embedding prediction within the conversion phase.

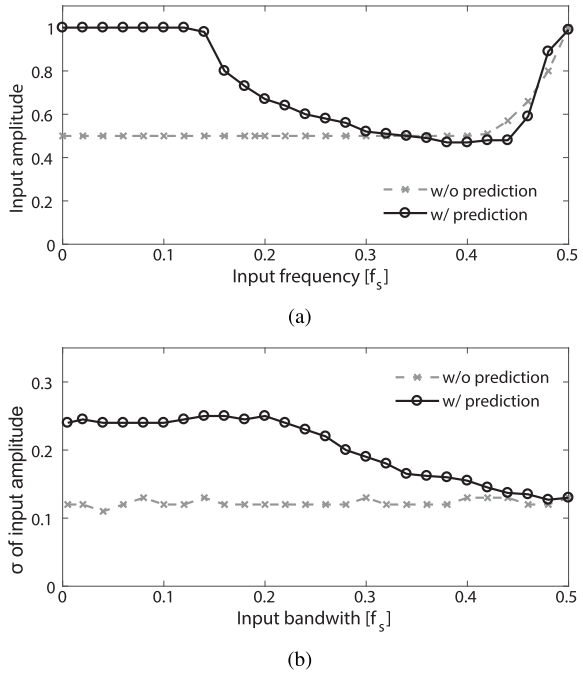

Fig. 13. Simulated input amplitude and frequency range supported by the proposed 1-bit 1st-order prediction with (a) sinusoidal and (b) Gaussian signals.

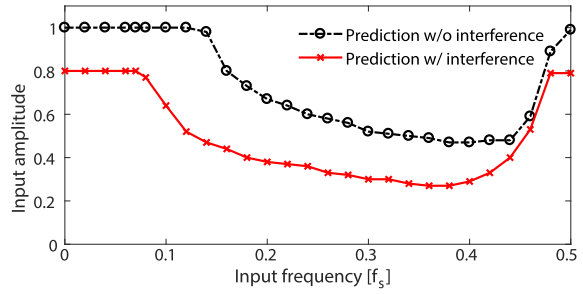

Fig. 14. Simulated input amplitude and frequency range supported by the proposed 1-bit 1st-order prediction with and without interference.

Fig. 13 shows the input amplitude and frequency range that the proposed prediction technique can support without signal overflow. It can be seen from Fig. 13(a) that the prediction works for a wide range of input amplitudes and frequencies. Even for full-scale sinusoidal input, the input frequency can be as high as $0.12f_s$, corresponding to an OSR of about 4, where f_s is the sampling rate. As will be shown later, the proposed prediction can be extended to high-order to support a small OSR of 2. Such a low requirement on OSR is satisfied by both Nyquist and oversampling applications.[2] When the input frequency goes beyond $0.12f_s$, the available input amplitude firstly decreases because the prediction error increases with input frequency, and then increases to full-scale at Nyquist frequency where $V_i(n)$ and $V_{LSB}(n-1)$ have the opposite polarity. The band-limited Gaussian random input signals are also tested. It can be seen from Fig. 13(b) that the proposed prediction can support a standard deviation $\sigma = 0.24$ for Gaussian random signals with a bandwidth of $[0, 0.2f_s]$ and $\sigma = 0.13$ for the full bandwidth of $[0, f_s/2]$. These results show that the proposed technique has only mild requirement on the input amplitude and frequency, and is generally applicable.

Note that the above discussion regarding the OSR requirement assumes no out-of-band interference. However, depending on the application, there could be strong interference, which can introduce additional prediction error. As shown in Fig. 11, the proposed technique has a prediction error tolerance of 0.75. This means that the total prediction error produced by both the in-band signal and the out-of-band interference has to be within this limit. Thus, the presence of strong out-of-band interference will reduce the allowable input signal swing and frequency range. Fig. 14 shows the simulated input amplitude and frequency range with and without out-of-band interference. The interference is assumed to be a

[2]The 1st-order and 2nd-order EF MESs are generally used for oversampling applications. For Nyquist converters, we can apply zeroth-order EF MES to randomize the mismatch error and turn them into white noise. The zeroth-order EF MES can be realized by feeding back the scrambled previous conversion codes.

Authorized licensed use limited to: Tsinghua University. Downloaded on February 21,2020 at 14:14:43 UTC from IEEE Xplore. Restrictions apply.

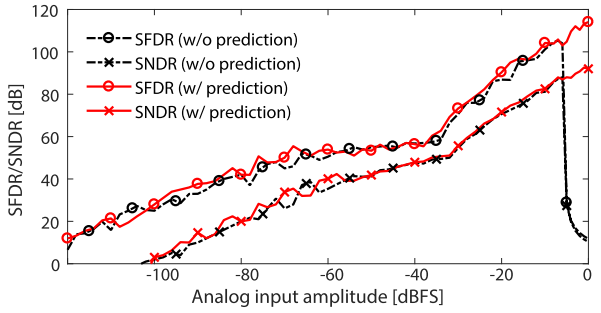

Fig. 15. Simulated SFDR/SDNR of a 16-bit SAR ADC with and without prediction, at 16× OSR.

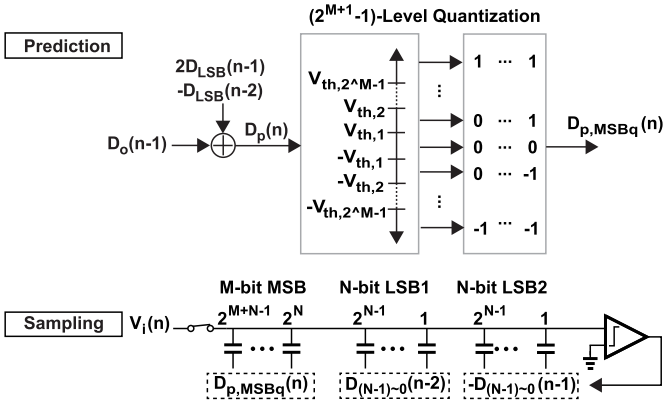

Fig. 16. Proposed multi-bit prediction for 2nd-order EF MES.

20% full-scale signal at $0.4f_s$. It shows that the maximum input amplitude is reduced to 80% full-scale, the frequency range that supports the maximum amplitude is reduced to $[0, 0.07f_s]$, corresponding to an OSR of 7. The interference issue requires extra attentions in a practical design.

Fig. 15 is the simulated SFDR and SNDR performance of a 16-bit SAR ADC with and without the proposed prediction, at 16 × OSR. It shows that when input amplitude is below −6 dBFS, the SFDR/SNDR lines before and after prediction match well. The key difference is that, without prediction, the input amplitude is limited to −6 dBFS. After enabling the prediction, the available input amplitude is increased to 0 dBFS. It proves that the proposed prediction can address the dynamic range loss issue without affecting the shaping capability of EF MES. Besides, the fluctuations on the SFDR/SNDR lines indicate the limited linearity enhancement capability of 1st-order EF MES.

B. Multi-Bit 1st-Order Prediction

For 2nd-order EF MES, the above mentioned prediction cannot be directly applied because a multi-bit (at least 2-bit) MSB DAC is required in the 2nd-order EF MES. Thus, the prediction output need to be multi-bit. Fig. 16 shows the prediction for 2nd-order EF MES with a M-bit MSB, in which the prediction signal D_p is given by

$$D_p(n) \equiv D_o(n-1) + 2D_{LSB}(n-1) - D_{LSB}(n-2). \quad (23)$$

A $(2^{M+1} - 1)$-level quantization is performed on D_p to obtain the M-bit prediction output $D_{p,MSBq}$. $D_{p,MSBq}$ is then applied to the M-bit MSB DAC in the sampling phase to reduce the effective input signal range. Similar with the analysis of Fig. 11, the optimal prediction thresholds those provide the largest prediction error tolerance can be found at

$$V_{th,i} = \frac{2i-1}{2^{M+1}+2}, \quad i \in [1, 2^M - 1]. \quad (24)$$

where i is the index of prediction threshold in Fig. 16.

Fig. 17(a) shows the input amplitude and frequency range that can be supported by the multi-bit 1st-order predictions for 2nd-order EF MES, with sinusoidal input signals. Without prediction, the input amplitude at low-frequency band is limited to 0.2 (−14 dBFS) with a 2-bit MSB, or is limited to 0.56 (−5.1 dBFS) with a 3-bit MSB. It is improved to a maximum of 0.8 (−1.9 dBFS) by prediction with 2-bit MSB. An interesting phenomenon is that the input amplitude can exceed the full-scale and the maximum amplitude is 4/3 (2.5 dBFS) when predicting with a 3-bit MSB. This is because the signal range subtracted from the MSB DAC by $D_{p,MSBq}$ (±7/9) is larger than that occupied by the LSB feedback (±3/9). The excess signal range (±4/9) can add up to the original analog input range (±8/9), leading to a maximum input range of ±4/3. The frequency range that supports the maximum signal swing is $[0, 0.06f_s]$ by the multi-bit prediction for 2nd-order EF MES, corresponding to an OSR of around 8. Comparing to Fig. 17, the input amplitude supported by multi-bit predictions does not increase at high-frequencies. The reason is that the injected LSB value $2D_{LSB}(n-1) - D_{LSB}(n-2)$ becomes small and random when with a multi-bit prediction, it cannot cancel the input amplitude at high frequencies. Besides, it can be seen from Fig. 17(b) that the 2-bit prediction can support a standard deviation $\sigma = 0.23$ for Gaussian random signals with a bandwidth of $[0, 0.1f_s]$ and $\sigma = 0.11$ for the full bandwidth of $[0, f_s/2]$. By the 3-bit prediction, the Gaussian random signals with a standard deviation $\sigma = 0.33$ in the frequency range of $[0, 0.12f_s]$, and $\sigma = 0.13$ for the full bandwidth of $[0, f_s/2]$ can be supported.

Fig. 18 shows the simulated SFDR/SDNR of a 16-bit SAR ADC with and without prediction, at 16× OSR. Without prediction, the input amplitude of the 2nd-order EF MES SAR ADC with a 2-bit MSB is limited to −14 dBFS. It is improved to −1.9 dBFS by prediction with the 2-bit MSB. By 3-bit prediction, the maximum input amplitude is 2.5 dBFS. Using larger bit of MSB DAC for prediction can lead to a larger extra dynamic range, but it is limited by the exponentially increased circuit complexity for an extra DEM.

C. General Form of Prediction

As discussed in Section IV-A and shown in Eq. (20), the 1st-order prediction provides the $1 - z^{-1}$ high-pass prediction error shaping, and can support a full-scale input in the frequency range of $[0, 0.12f_s]$. To extend the supported input frequency range for Nyquist applications, high-order prediction techniques can be used. By approximating V_i with $2D_o(n-1) - D_o(n-2)$, the prediction error can be 2nd-order shaped with $(1 - z^{-1})^2$. Similarly, the 3rd-order $(1 - z^{-1})^3$

Authorized licensed use limited to: Tsinghua University. Downloaded on February 21,2020 at 14:14:43 UTC from IEEE Xplore. Restrictions apply.

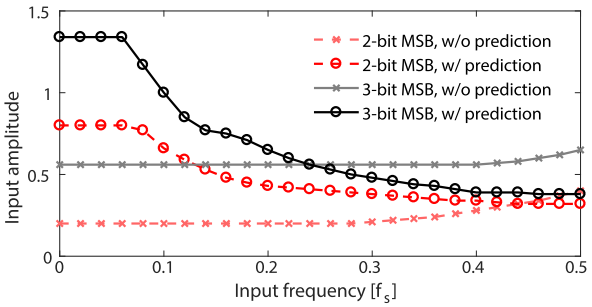

(a)

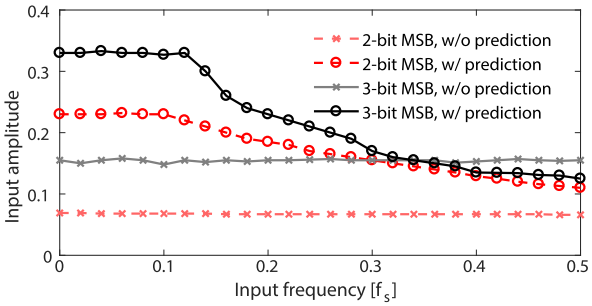

(b)

Fig. 17. Simulated input amplitude and frequency range supported by the multi-bit 1st-order prediction with (a) sinusoidal and (b) Gaussian signals.

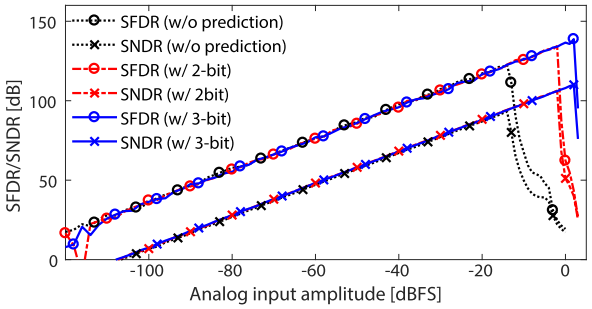

Fig. 18. Simulated SFDR/SDNR of a 16-bit SAR ADC at 16× OSR: without prediction, with 2-bit prediction and with 3-bit prediction.

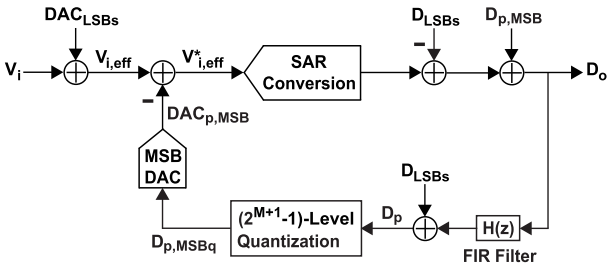

Fig. 19. Proposed general form of prediction for EF MES.

prediction error shaping can be realized by using $3D_o(n-1)-3D_o(n-2)+D_o(n-3)$. In addition, the prediction techniques for high-pass and band-pass signal processing can also be generalized. For example, the $1+z^{-1}$ prediction provides the prediction error shaping at $f_s/2$, and the $1+z^{-2}$ prediction provides the bandpass shaping at $f_s/4$.

Based on the discussion above, the general form of prediction can be reached, as shown in Fig. 19. Different from the 1st-order prediction in Fig. 10, a finite-impulse-response (FIR) filter is applied on D_o to approximate V_i for achieving various

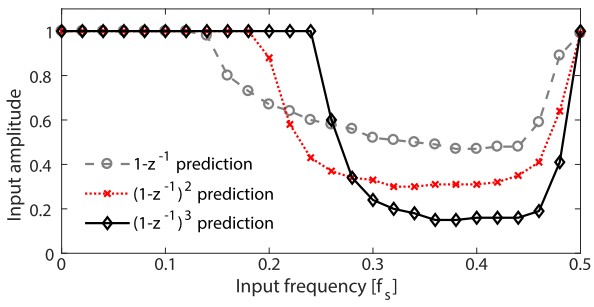

(a)

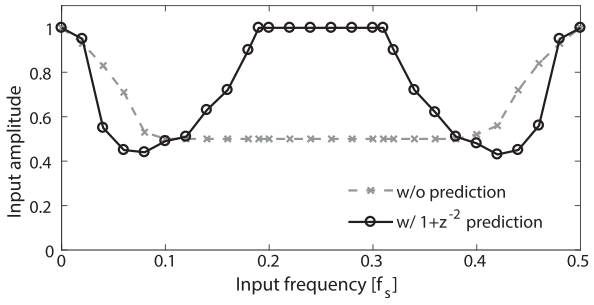

(b)

Fig. 20. Simulated sinusoidal input amplitude versus frequency by (a) $1-z^{-1}$, $(1-z^{-1})^2$, $(1-z^{-1})^3$ predictions with $1-z^{-1}$ EF MES and (b) $1+z^{-2}$ prediction with $1+z^{-2}$ EF MES.

prediction error shaping effects. The transfer function of the FIR filter is given by

$$H(z) = -c_{p,1}z^{-1} - c_{p,2}z^{-2} - \cdots - c_{p,k}z^{-k} \tag{25}$$

Comparing to the general form of EF MES, the coefficient $c_{p,i}$ for $H(z)$ has no restriction because it is realized in the digital domain.

The general form of prediction signal is given by

$$D_p(z) = H(z)D_o + D_{LSBs} \tag{26}$$

where D_{LSBs} is the sum of weights of previous LSB feedback. The general form of shaped prediction error is given by

$$\begin{aligned} E_p(z) &\equiv V_{i,eff}(z) - D_p(z) \\ &\approx V_i(z)\cdot(1 + c_{p,1}z^{-1} + c_{p,2}z^{-2} + \cdots + c_{p,k}z^{-k}) \end{aligned} \tag{27}$$

Like the case of 2nd-order EF MES, depending on the signal range occupied by D_{LSBs}, a multi-bit (M-bit) MSB may be necessary. If so, D_p has to be re-quantized to M-bit to apply to the MSB DAC. With a M-bit prediction, the signal swing compensated by the MSB DAC is

$$A_p = \frac{2^M - 1}{2^M - 1 + k^*}. \tag{28}$$

Combining equation (28) with equations (13) and (14), the maximum available input signal swing provided by a M-bit prediction can be obtained as

$$\begin{aligned} A_{in} &= A_{max} + A_p - A_{LSB} \\ &= \frac{2^{M+1} - 1 - \sum_{i=1}^{k} |c_i|}{2^M + k^* - 1}. \end{aligned} \tag{29}$$

Authorized licensed use limited to: Tsinghua University. Downloaded on February 21,2020 at 14:14:43 UTC from IEEE Xplore. Restrictions apply.

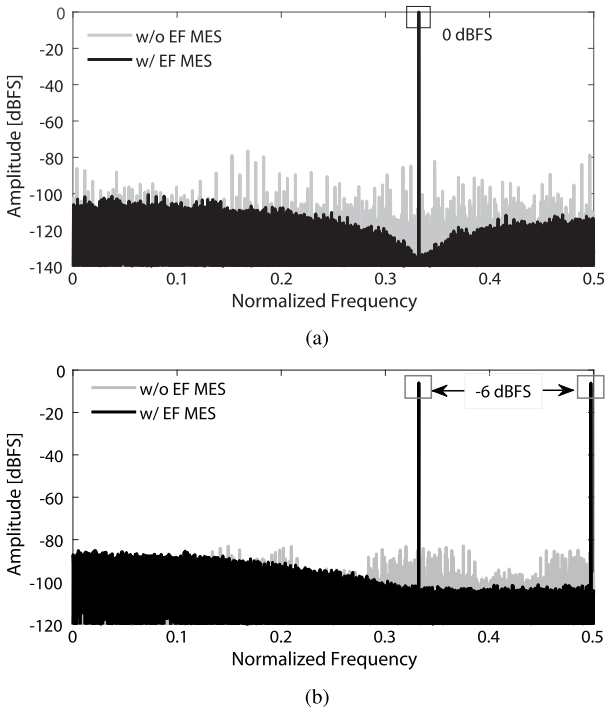

Fig. 21. Output spectra of 16-bit SAR ADCs with (a) $1+z^{-1}+z^{-2}$ EF MES and 2-bit $1+z^{-1}+z^{-2}$ prediction, (b) $1+2z^{-1}+2z^{-2}+z^{-3}$ EF MES and 3-bit $1+2z^{-1}+2z^{-2}+z^{-3}$ prediction.

Accordingly, the minimum number of MSB bits that supports the full-scale input signal is determined by

$$M \geq \log_2(\sum_{i=1}^{k} |c_i| + k^*) \tag{30}$$

It ensures the signal range occupied by D_{LSBs} can be completely canceled out by $DAC_{p,MSB}$, so that A_{in} can achieve the full-scale ($A_{in} \geq 1$).

Fig. 20(a) shows the simulated input amplitude and frequency range supported by high-order predictions, and compares them to that by the 1st-order prediction in the context of a SAR ADC with the 1st-order $1-z^{-1}$ EF MES. It shows that the 2nd-order and 3rd-order predictions can extend the input frequency that supporting full-scale input to $0.18f_s$ and $0.24f_s$, corresponding to $2.8\times$ OSR and $2\times$ OSR, respectively. The high-order predictions improve the prediction accuracy and extend the input frequency range significantly.

Fig. 20 shows the simulated input amplitude and frequency range by $1+z^{-2}$ prediction for a band-pass SAR ADC with $1+z^{-2}$ EF MES. It shows that the $1+z^{-2}$ prediction achieves the prediction error shaping at $f_s/4$, the full-scale input frequency range is $[0.19f_s, 0.31f_s]$.

The proposed general forms of EF MES and prediction can provide the general solutions for designing complex forms of mismatch shaping and addressing the dynamic range loss issue. To demonstrate the usefulness, two simulated output spectra of bandpass SAR ADCs are provided in Fig. 21. Fig. 21(a) is the output spectrum of a 16-bit SAR ADC with $1+z^{-1}+z^{-2}$ EF MES using a 2-bit MSB and two 14-bit LSB DACs. The corresponding 2-bit $1+z^{-1}+z^{-2}$ prediction is performed to address the dynamic range loss. The output spectrum shows the mismatch shaping effect at the frequency of $f_s/3$. Owing to the prediction, it can operate with a maximum input signal swing of 0 dBFS, which is consistent with the analysis result by equation (29).

A more complex $1+2z^{-1}+2z^{-2}+z^{-3}$ EF MES is realized by using a 3-bit MSB DAC and three 13-bit LSB DACs, it achieves the mismatch shaping at both $f_s/3$ and $f_s/2$, as shown in Fig. 21(b). The 3-bit $1+2z^{-1}+2z^{-2}+z^{-3}$ prediction is applied to make it operate with a full-scale two-tone input.

V. Conclusion

This paper presents a comprehensive study of EF MES and proposes several novel techniques to address the limitations of the prior EF MES technique. It systematically generalizes EF MES to 2nd-order shaping and general form, enabling it to be applied to various types of low-pass, band-pass and high-pass ADCs and DACs. Moreover, this paper addresses the critical dynamic range loss problem by digital prediction.

Different from the DEM based MES, the EF MES has lower complexity and can directly work with power-of-two-weighted DAC elements. As a result, it is especially well suited for high-resolution data converters. It can serve as an attractive alternative to calibration and DEM techniques to handle mismatch errors and improve linearity.

References

[1] H.-S. Lee, D. A. Hodges, and P. R. Gray, "A self-calibrating 15 bit CMOS A/D converter," *IEEE J. Solid-State Circuits*, vol. SSC-19, no. 6, pp. 813–819, Dec. 1984.

[2] R. T. Baird and T. S. Fiez, "A low oversampling ratio 14-b 500-kHz $\Delta\Sigma$ ADC with a self-calibrated multibit DAC," *IEEE J. Solid-State Circuits*, vol. 31, no. 3, pp. 312–320, Mar. 1996.

[3] U.-K. Moon, J. Silva, J. Steensgaard, and G. C. Temes, "Switched-capacitor DAC with analogue mismatch correction," *Electron. Lett.*, vol. 35, no. 22, pp. 1903–1904, Oct. 1999.

[4] I. Galton, "Digital cancellation of D/A converter noise in pipelined A/D converters," *IEEE Trans. Circuits Syst. II, Analog Digit. Signal Process.*, vol. 47, no. 3, pp. 185–196, Mar. 2000.

[5] N. Sun, H. S. Lee, and D. Ham, "Digital background calibration in pipelined ADCs using commutated feedback capacitor switching," *IEEE Trans. Circuits Syst. II, Exp. Briefs*, vol. 55, no. 9, pp. 877–881, Sep. 2008.

[6] K. Ragab, L. Chen, A. Sanyal, and N. Sun, "Digital background calibration for pipelined ADCs based on comparator decision time quantization," *IEEE Trans. Circuits Syst. II, Exp. Briefs*, vol. 62, no. 5, pp. 456–460, May 2015.

[7] R. J. V. D. Plassche, "Dynamic element matching for high-accuracy monolithic D/A converters," *IEEE J. Solid-State Circuits*, vol. SSC-11, no. 6, pp. 795–800, Dec. 1976.

[8] B. H. Leung and S. Sutarja, "Multibit $\Sigma-\Delta$ A/D converter incorporating a novel class of dynamic element matching techniques," *IEEE Trans. Circuits Syst. II, Analog Digit. Signal Process.*, vol. 39, no. 1, pp. 35–51, Jan. 1992.

[9] H. S. Jackson, "Circuit and method for cancelling nonlinearity error associated with component value mismatches in a data converter," U.S. Patent 5 221 926, Jun. 22, 1993.

[10] R. W. Adams and T. W. Kwan, "Data-directed scrambler for multi-bit noise shaping D/A converters," U.S. Patent 5 404 142, Apr. 4, 1995.

[11] R. T. Baird and T. S. Fiez, "Linearity enhancement of multibit $\Delta\Sigma$ A/D and D/A converters using data weighted averaging," *IEEE Trans. Circuits Syst. II, Analog Digit. Signal Process.*, vol. 42, no. 12, pp. 753–762, Dec. 1995.

[12] R. Schreier and B. Zhang, "Noise-shaped multibit D/A convertor employing unit elements," *Electron. Lett.*, vol. 31, no. 20, pp. 1712–1713, Sep. 1995.

Authorized licensed use limited to: Tsinghua University. Downloaded on February 21,2020 at 14:14:43 UTC from IEEE Xplore. Restrictions apply.

[13] I. Galton, "Spectral shaping of circuit errors in digital-to-analog converters," *IEEE Trans. Circuits Syst. II, Analog Digit. Signal Process.*, vol. 44, no. 10, pp. 808–817, Oct. 1997.
[14] N. Sun and P. Cao, "Low-complexity high-order vector-based mismatch shaping in multibit $\Delta\Sigma$ ADCs," *IEEE Trans. Circuits Syst. II, Exp. Briefs*, vol. 58, no. 12, pp. 872–876, Dec. 2011.
[15] N. Sun, "High-order mismatch-shaping in multibit DACs," *IEEE Trans. Circuits Syst. II, Exp. Briefs*, vol. 58, no. 6, pp. 346–350, Jun. 2011.
[16] A. Sanyal and N. Sun, "Dynamic element matching techniques for static and dynamic errors in continuous-time multi-bit $\Delta\Sigma$ modulators," *IEEE J. Emerg. Sel. Topics Circuits Syst.*, vol. 5, no. 4, pp. 598–611, Dec. 2015.
[17] J. Remple and I. Galton, "The effects of inter-symbol interference in dynamic element matching DACs," *IEEE Trans. Circuits Syst. I, Reg. Papers*, vol. 64, no. 1, pp. 14–23, Jan. 2017.
[18] J. A. Fredenburg and M. P. Flynn, "A 90-MS/s 11-MHz-bandwidth 62-dB SNDR noise-shaping SAR ADC," *IEEE J. Solid-State Circuits*, vol. 47, no. 12, pp. 2898–2904, Dec. 2012.
[19] Z. Chen, M. Miyahara, and A. Matsuzawa, "A 9.35-ENOB, 14.8 fJ/conv.-step fully-passive noise-shaping SAR ADC," in *Proc. IEEE Symp. VLSI Circuits*, Jun. 2015, pp. C64–C65.
[20] W. Guo and N. Sun, "A 12b-ENOB 61 μW noise-shaping SAR ADC with a passive integrator," in *Proc. IEEE Eur. Solid-State Circuits Conf.*, Sep. 2016, pp. 405–408.
[21] Y.-S. Shu, L.-T. Kuo, and T.-Y. Lo, "An oversampling SAR ADC with DAC mismatch error shaping achieving 105 dB SFDR and 101 dB SNDR over 1 kHz BW in 55 nm CMOS," *IEEE J. Solid-State Circuits*, vol. 51, no. 12, pp. 2928–2940, Dec. 2016.
[22] K. Obata, K. Matsukawa, T. Miki, Y. Tsukamoto, and K. Sushihara, "A 97.99 dB SNDR, 2 kHz BW, 37.1 μW noise-shaping SAR ADC with dynamic element matching and modulation dither effect," in *Proc. IEEE Symp. VLSI Circuits (VLSI-Circuits)*, Honolulu, HI, USA, Jun. 2016, pp. 1–2.
[23] C.-C. Liu and M.-C. Huang, "A 0.46 mW 5 MHz-BW 79.7 dB-SNDR noise-shaping SAR ADC with dynamic-amplifier-based FIR-IIR filter," in *IEEE ISSCC Dig. Tech. Papers*, Feb. 2017, pp. 466–467.
[24] W. Guo, H. Zhuang, and N. Sun, "A 13 b-ENOB 173 dB-FoM 2^{nd}-order NS SAR ADC with passive integrators," in *IEEE Symp. VLSI Circuits Dig. Tech. Papers*, Jun. 2017, pp. 236–237.
[25] S. Li, B. Qiao, M. Gandara, and N. Sun, "A 13-ENOB 2^{nd}-order noise-shaping SAR ADC realizing optimized NTF zeros using an error-feedback structure," in *IEEE ISSCC Dig. Tech. Papers*, Feb. 2018, pp. 234–236.
[26] R. Adams and K. Q. Nguyen, "A 113-dB SNR oversampling DAC with segmented noise-shaped scrambling," *IEEE J. Solid-State Circuits*, vol. 33, no. 12, pp. 1871–1878, Dec. 1998.
[27] K. L. Chan and I. Galton, "A 14 b 100 MS/s DAC with fully segmented dynamic element matching," in *IEEE ISSCC Dig. Tech. Papers*, Feb. 2006, pp. 2390–2399.
[28] K. L. Chan, J. Zhu, and I. Galton, "Dynamic element matching to prevent nonlinear distortion from pulse-shape mismatches in high-resolution DACs," *IEEE J. Solid-State Circuits*, vol. 43, no. 9, pp. 2067–2078, Sep. 2008.
[29] Z. Zhang and G. C. Temes, "A segmented data-weighted-averaging technique," in *Proc. IEEE Int. Symp. Circuits Syst.*, May 2007, pp. 481–484.
[30] K. L. Chan, N. Rakuljic, and I. Galton, "Segmented dynamic element matching for high-resolution digital-to-analog conversion," *IEEE Trans. Circuits Syst. I, Reg. Papers*, vol. 55, no. 11, pp. 3383–3392, Dec. 2008.
[31] N. Sun, "High-order mismatch-shaped segmented multibit $\Delta\Sigma$ DACs with arbitrary unit weights," *IEEE Trans. Circuits Syst. I, Reg. Papers*, vol. 59, no. 2, pp. 295–304, Feb. 2012.
[32] J. Liu, G. Wen, and N. Sun, "Second-order DAC MES for SAR ADCs," *Electron. Lett.*, vol. 53, no. 24, pp. 1570–1572, Oct. 2017.
[33] I. Fujimori *et al.*, "A 90-dB SNR 2.5-MHz output-rate ADC using cascaded multibit delta-sigma modulation at 8× oversampling ratio," *IEEE J. Solid-State Circuits*, vol. 35, no. 12, pp. 1820–1828, Dec. 2000.
[34] D.-H. Lee and T.-H. Kuo, "Advancing data weighted averaging technique for multi-bit Sigma–Delta modulators," *IEEE Trans. Circuits Syst. II, Exp. Briefs*, vol. 54, no. 10, pp. 838–842, Oct. 2007.
[35] J. Welz, I. Galton, and E. Fogleman, "Simplified logic for first-order and second-order mismatch-shaping digital-to-analog converters," *IEEE Trans. Circuits Syst. II, Analog Digit. Signal Process.*, vol. 48, no. 11, pp. 1014–1027, Nov. 2001.
[36] K. C.-H. Chiang, N. S. Artan, and H. J. Chao, "A signal-specific approach for reducing SAR-ADC power consumption," in *Proc. IEEE Biomed. Circuits Syst. Conf. (BioCAS)*, Oct. 2013, pp. 278–281.
[37] N. Wood and N. Sun, "Predicting ADC: A new approach for low power ADC design," in *Proc. IEEE Dallas Circuits Syst. Conf.*, Oct. 2014, pp. 1–4.

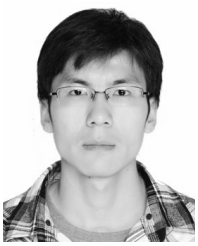

Jiaxin Liu (S'13) received the B.S. degree from Shandong University, Jinan, China, in 2010, and the M.S. and Ph.D. degrees from the University of Electronic Science and Technology of China (UESTC), Chengdu, China, in 2013 and 2018, respectively. He was a visiting Ph.D. student with the Department of Electrical and Computer Engineering, The University of Texas at Austin, Austin, TX, USA, from 2015 to 2017. He is currently a Post-Doctoral Researcher with Tsinghua University, Beijing, China.

Dr. Liu received the First Prize of Academic Scholarship in UESTC for the consecutive years from 2012 to 2015, the China National Scholarship in 2012, the First Prize of VeriSilicon Circuits Design Competition in 2015, and the China CSC Scholarship in 2015.

His current research interests are power-efficient data converters, especially SAR-based hybrid ADCs, and mismatch error shaping techniques. His broad research interests include RF, analog, and mixed-signal integrated circuits design.

Chen-Kai Hsu (S'15) was born in Changhua, Taiwan, in 1991. He received the B.S. degree in electrical engineering from National Chung Cheng University, Chiayi, Taiwan, in 2012, and the M.S. degree in electronics engineering from National Taiwan University, Taipei, Taiwan, in 2015. He is currently pursuing the Ph.D. degree with The University of Texas at Austin.

His current research focuses on high-performance data converters. His broader research interests include mixed signal and analog IC design.

Xiyuan Tang (S'17) received the B.Sc. degree (Hons.) from the School of Microelectronics, Shanghai Jiao Tong University, Shanghai, China, in 2012, and the M.S. degree in electrical engineering from The University of Texas at Austin, Austin, TX, USA, where he is currently pursuing the Ph.D. degree.

He was a Design Engineer with Silicon Laboratories, Austin, where he was involved in receiver design. His research interests include digitally assisted data converters, low-power mixed-signal circuits, and analog data processing.

Mr. Tang received the National Scholarship in China in 2011.

Shaolan Li (S'12) received the B.Eng. degree (Hons.) from The Hong Kong University of Science and Technology, Hong Kong, in 2012, where he ranked top in the Electronic and Computer Engineering Department. He is currently pursuing the Ph.D. degree with The University of Texas at Austin, Austin, TX, USA.

In 2013, he was an Intern with the WLAN-RF Group, Broadcom Ltd., Sunnyvale. In Fall 2014, he interned at Freescale, Tempe, where he was involved in designing ADC for automobile MCU. His current research interests include low-power scaling-friendly oversampling data converter design techniques, synthesizable mixed-signal circuits, and sensor interfaces, with a special focus on VCO-based ADCs and noise-shaping SAR ADCs. His research has resulted in several publications in JSSC, ISSCC, VLSI Symposium, and ESSCIRC.

Mr. Li received the Academic Achievement Medal from HKUST in 2012, the HKUST Undergraduate Scholarship in 2012, the UT Austin Cockrell School of Engineering Fellowship in 2017, and the IEEE SSCS Pre-Doctoral Achievement Award from 2017 to 2018. He serves as a Reviewer for the IEEE TCAS-I and IEEE TCAS-II.

Authorized licensed use limited to: Tsinghua University. Downloaded on February 21,2020 at 14:14:43 UTC from IEEE Xplore. Restrictions apply.

Guangjun Wen (M'04–SM'10) received the B.S. and M.E. degrees from Chongqing University, Chongqing, China, in 1986 and 1992, respectively, and the Ph.D. degree from the University of Electronic Science and Technology of China (UESTC), Chengdu, China, in 1998. From 1986 to 1995, he was with Chongqing University, as a Lecturer. He was with UESTC, from 1998 to 2000, and then with the Electronics and Telecommunication Research Institute, South Korea, from 2000 to 2001, as a Post-Doctoral Fellow. He was with Nanyang Technological University, Singapore, as a Research Fellow, from 2001 to 2002. He worked for VS Electronic Pte Ltd, Singapore, and the Sumitomo Electric Group, Yokohama, Japan, as a Senior RF Design Engineer from 2002 to 2005. Since 2004, he has been a Full Professor with UESTC.

He has authored or co-authored more than 200 journal papers and presented more than 120 conference papers. His research interests are in radio frequency integrated circuits and systems for various wireless communication systems, RFID tag and reader, circuit components, and antennas design for the Internet of Things.

Nan Sun (S'06–M'11–SM'16) received the B.S. degree from Tsinghua University, Beijing, China, in 2006, where he ranked top in the Department of Electronic Engineering, and the Ph.D. degree from the School of Engineering and Applied Sciences, Harvard University, Cambridge, MA, USA, in 2010.

He is currently an Associate Professor with the Department of Electrical and Computer Engineering, The University of Texas (UT) at Austin, Austin, TX, USA. His current research interests include analog, mixed- signal, and RF integrated circuits, miniature spin resonance systems, magnetic sensors and image sensors, and micro- and nano-scale solid-state platforms (silicon ICs and beyond) to analyze biological systems for biotechnology and medicine.

Dr. Sun received the NSF Career Award in 2013 and the Jack Kilby Research Award from UT at Austin in 2015 and 2016. He holds the AMD Endowed Development Chair from 2013 to 2017. He serves on the Technical Program Committee of the IEEE Custom Integrated Circuits Conference and the IEEE Asian Solid-State Circuit Conference. He is an Associate Editor of the IEEE TRANSACTIONS ON CIRCUITS AND SYSTEMS I, Regular Papers and a Guest Editor of the IEEE JOURNAL OF SOLID-STATE CIRCUITS.

Authorized licensed use limited to: Tsinghua University. Downloaded on February 21,2020 at 14:14:43 UTC from IEEE Xplore. Restrictions apply.